Structure of the Electrical Double Layer Revisited: Electrode Capacitance in Aqueous Solutions

Mahmoud Khademi and Dominik P. J. Barz*

Department of Chemical Engineering, Queen's University, Kingston, ON, K7L 3N6, Canada

E-mail: dominik.barz@queensu.ca

Abstract

The structure of the electrical double layer at the interface of planar electrodes and aqueous solutions is investigated. Electrical impedance spectroscopy is used to measure the impedance of aqueous solutions of sodium chloride and two different surfactants over a wide range of concentrations. The electrode capacitance is directly inferred from the admittance spectra, as well as by regression of the impedance spectra to an equivalent circuit. It is found that the electrode capacitance remains on the same order of magnitude over the entire range of investigated concentrations. This is contradictive to the predictions of the Gouy-Chapman-Stern theory which predicts that at low concentrations, the electrode capacitance should be determined by the diffuse layer. It is concluded that the Stern layer capacitance always dominates the electrode capacitance, even at very low concentrations, and the establishment of a diffuse layer capacitance

requires an ionic strength of around 1 mM.

Keywords

Electrical Double Layer, Stern Layer, Diffuse Layer, Surfactant, Electrical Impedance Spectroscopy

Introduction

The term Electrical Double Layer (EDL) refers to an interface of a charged surface and a liquid where the electro-neutrality is violated and an electric field exists. As a result, ions and/or dipole molecules in the liquid phase change their location and orientation to diminish the effect of the electric field.[1–3] Separation of electric charges in an EDL can be compared to the behavior of a capacitor in an electrical circuit; which is indeed practically utilized in EDL supercapacitors.[4,5] Hence, researchers generally model the EDL properties as a capacitor in order to investigate electric charges at the interface and the properties of the EDL.[1,2,6]

The first and simplest model of an EDL was proposed by Helmholtz in 1879.[7] He assumed that at the interface of a charged surface and an electrolyte, there is an immobile layer of "adsorbed", solvated ions of opposite charge. In this model, the EDL acts like a single conventional parallel-plate capacitor.[8] Later in the early 1900s, Gouy and Chapman independently developed the diffuse layer EDL theory. In the so-called Gouy-Chapman (GC) model, charges are assumed to be mobile. They do not "adsorb" on the charged surface since the electrostatic attraction is balanced by the thermal energy (diffusion). Therefore, the ion concentration exponentially changes over the so-called Debye length which is considered as the approximate thickness of the EDL.[6,8] The GC model does not account for the ion size and assumes point like charges which have no limitation of approaching the surface.[2] Stern in 1920 combined the concepts of Helmholtz and GC models, and proposed that an EDL comprises of an immobile Stern (SL) and a mobile diffuse layer (DL). This model is therefore called the Gouy-Chapman-Stern (GCS) model.[2,6] In 1947, Graham refined the Stern model by dividing the Stern layer into two subregions, the inner Helmholtz (IHP) and the outer Helmholtz (OHP) plane (layer). The location of the IHP is defined as the center of the specifically adsorbed ions; i.e., ions which lost their solvation shell and are as close as possible to the surface. In contrast, the position of the OHP is the location of the center of the solvated ions closest to the surface.[1] Later on, Bockris et al.[9] considered the influence

of the electric field on the solvent (water) molecules in the SL. In the IHP, the influence of the electric field is very pronounced so that the solvent molecules orientate, depending on the surface charge, with the field direction. In the OHP (and the DL), the solvent molecules orientate towards the solvated ion. This difference results in variations in the dielectric permittivity of each region.[9] From an experimental point of view, it is more pragmatic to assume that the EDL is a combination of the immobile SL and the mobile DL with different permittivities.[10]

There are numerous studies reporting the EDL capacitance for different conditions.[1,11–22] However, to the best of our knowledge, there is no systematic experimental study which covers a wide range of concentration of aqueous solutions, especially very low concentrations, and which accounts for the permittivity difference between the SL and the DL. The most common analytical techniques used to determine the EDL capacitance are cyclic voltammetry and electrical (electrochemical) impedance spectroscopy (EIS). The latter is preferred in our work since it analyses the EDL behavior over a wide range of (excitation) timescales. Moreover, EIS can be performed with a very small excitation signal and, therefore, a linear relationship between voltage and current can be assumed.[23]

In this study we obtain the overall capacitance of an EDL from EIS measurements using different evaluation strategies. That is, by interpretation of an equivalent electrical circuit which is fitted to the impedance spectra, as well as by direct calculation from admittance and complex capacitance spectra. In contrast to the work of others, we investigate a wide range of ion concentrations and focus specifically on very low ion ionic strength liquids. To the best of our knowledge, this is a regime where EIS has not been used and, thus, there is a lack of experimental data and their interpretation. In addition, we resolve the structure of the EDL by adequately dividing the measured capacitance into the Stern and diffuse layer capacitances. The system to be investigated are aqueous solutions of the simple electrolyte sodium chloride (NaCl). Additionally, we investigate aqueous solutions

of the anionic surfactant sodium dodecyl sulfate (SDS) and the zwitterionic surfactant 3-(N,N-Dimethylmyristylammonio)propanesulfonate (TDAPS). The simple electrolyte is chosen because the small size of the ions. This allows us to assume that the respective EDL can be adequately described with the Gouy-Chapman-Stern model. The motivation for the surfactants is their relatively large size which should prevent the establishment of the DL or at least diminish its influence. This should be especially true for the zwitterionic surfactant due to the lack of a net charge.

This article continues with a brief theory of EIS. Then, the experimental methodology and materials are discussed. Subsequently, the experimental findings are presented where we also describe the different methods to infer the EDL capacitance from impedance, admittance and the complex capacitance spectra. The discussion continues with a scaling analysis that we apply to identify the dominant capacitance in a certain range of concentrations. Finally, this article ends with a summary section.

Theory

In this section, a brief theory of EIS is provided. The electrical impedance $Z(\omega)$ at an angular frequency ω is the ratio of the applied AC potential difference $V(\omega)$ to the AC current $I(\omega)$. It is composed of a real $Z^{'}(\omega)$ and an imaginary $Z^{''}(\omega)$ part according to

$$Z(\omega) = \frac{V(\omega)}{I(\omega)} = Z^{'}(\omega) + jZ^{''}(\omega), \tag{1}$$

where j is the imaginary unit.[24] Similar to the relationship between electrical resistivity and conductivity, we can define the electrical admittance

$$Y(\omega) = \frac{1}{Z(\omega)} = Y^{'}(\omega) + jY^{''}(\omega), \tag{2}$$

where $Y^{'} = \frac{Z^{'}}{Z^{'2}+Z^{''2}}$ is the real part and $Y^{''} = -\frac{Z^{''}}{Z^{'2}+Z^{''2}}$ is the imaginary part of the admittance.[24] If we use the impedance of a single capacitor $Z = 1/j\omega C$, the complex capacitance can be written as

$$C(\omega) = \frac{1}{j\omega Z(\omega)} = \frac{Y(\omega)}{j\omega} = C^{'}(\omega) - jC^{''}(\omega). \tag{3}$$

Accordingly, the real and the imaginary part of the complex capacitance are $C^{'} = -\frac{Z^{''}}{\omega(Z^{'2}+Z^{''2})}$ and $C^{''} = \frac{Z^{'}}{\omega(Z^{'2}+Z^{''2})}$, respectively.[25] Note that an implication of this definition is that the entire (measurement) cell is considered as a single capacitor. We show below that this assumption, despite its simplicity, gives very accurate results.

As it can be concluded from Equations (1)–(3), the concepts of impedance, admittance and complex capacitance can be converted into each other. For a known capacitor geometry (surface area and electrode distance), we can also infer the electrical resistivity, conductivity and permittivity at each frequency. The choice of the data representation – impedance, admittance or complex capacitance – is usually based on the system or the parameter of interest. For example, impedance spectra are usually preferred in an electrochemical context since it elucidates the information on the resistive and reactive behavior of a system. In contrast, admittance and complex capacitance representations are helpful when the focus is on the capacitive behavior of a system.[24]

As mentioned above, the main focus of this work is to measure the EDL capacitance of an electrode. Here, we employ three different methods: (i) We use equivalent (electrical) circuits which consist of multiple linear and nonlinear elements and fit them to the measured impedance spectra. This method is considered the most accurate in determining the behavior of an electrochemical system.[24] However, the dilemma of this method is that it relies on multivariable regression and adequate regression qualities can be achieved with very different equivalent circuits. In other words, a good fit does not necessarily reflect a correct physicochemical description of the system. Thus, the most appropriate equivalent circuit must be

carefully chosen and validated. We discuss the equivalent circuits that we use in this work below. (ii) To validate the values inferred from equivalent circuits, we also directly determine the EDL capacitance based on the admittance (capacitance) spectra. This method is based on the assumption of an ideal capacitive behavior of an EDL, which is manifested as a relaxation process at low excitation frequencies.[24] From the time constant of this relaxation frequency, the value of the EDL capacitance is estimated. (iii) Likewise, assuming that the entire cell is reasonably-well described as an ideal capacitor allows for approximation of the EDL capacitance from the real part of the complex capacitance. We show in the Results and Discussion section that despite the simplifications assumed in methods (ii) and (iii), we achieve very consistent values for the EDL capacitance.

Experimental Section

In this section, we introduce the chemicals, materials, and experimental setup that are used for this work.

Chemicals

Sodium chloride (NaCl, $\geq$99.5%, Sigma-Aldrich, Canada), anionic sodium dodecyl sulfate, SDS ($NaC_{12}H_{25}SO_4$, $\geq$95.0%, MP Biomedicals, LLC, France) and zwitterionic 3-(*N*,*N*-dimethylmyristylammonio)propanesulfonate, TDAPS ($C_{19}H_{41}NO_3S$, $\geq$98.0%, Fluka, Switzerland), are used to prepare the electrolyte solutions. All solutions are made with deionized (DI) water with a conductivity of < 1 μS/cm from an RiOs–DI3 water purification system (Millipore Sigma, Etobicoke, Canada).

Experimental Setup

To conduct the EIS measurements, a custom made parallel-plate cell is used. The electrodes (non-alkaline grade, University Wafer, U.S.A.) are made from boro-aluminosilicate glass with a coated layer of indium tin oxide (ITO) featuring a surface conductivity of 10–15 Ω/sq. Two polymeric distance holders are printed using a Miicraft+ 3D printer (Miicraft, Hsinchu, Taiwan). The holders allow for wires to be guided through holes to enable electrical contact with the electrodes before assembling the cell. After assembly, the holders keep the electrodes apart with a distance of 2 mm and also establish the tight contact between wires and electrodes. The so-assembled cell is placed in a petri dish and then the respective liquid sample is added.

All EIS measurements are carried out using a potentiostat/galvanostat (Autolab PG-STAT302N, Metrohm Autolab B.V., Netherlands). The frequency range of the measurements varies depending on the sample within a range of 1 MHz to 10 mHz. The measurements are performed at open circuit by a superposition of a sinusoidal AC voltage with an amplitude of 10 mV. Each measurement is repeated at least three times to ensure the reproducibility of the results as well as to allow for calculation of the standard deviation. The regressions of the spectra are carried out using the software NOVA 1.11 (Metrohm Autolab B.V., Netherlands). To verify the EIS-based methodology, additional cyclic voltammetry (CV) measurements are performed using the same custom-made measurement cell. These CV measurements are conducted with terminal potentials of -0.1 and 0.1 V and with a scan rate of 10 mV/s.

Results and Discussion

In this section, we present our experimental findings and discuss the results based on the different theories that we apply to identify the different processes involved in our system.

Impedance Spectra and Fitting

Figures 1a and b give the Nyquist plots of solutions with a low concentration of 10 μM as well as a high concentration of 100 mM of NaCl, SDS or TDAPS in DI water. In addition, the Nyquist diagram of a pure DI water sample is also included in Figure 1a. Experimental results are given as symbols, while results from the equivalent circuit regression are shown as solid line. The respective values of the circuit elements are presented in the Supporting Information to this article.

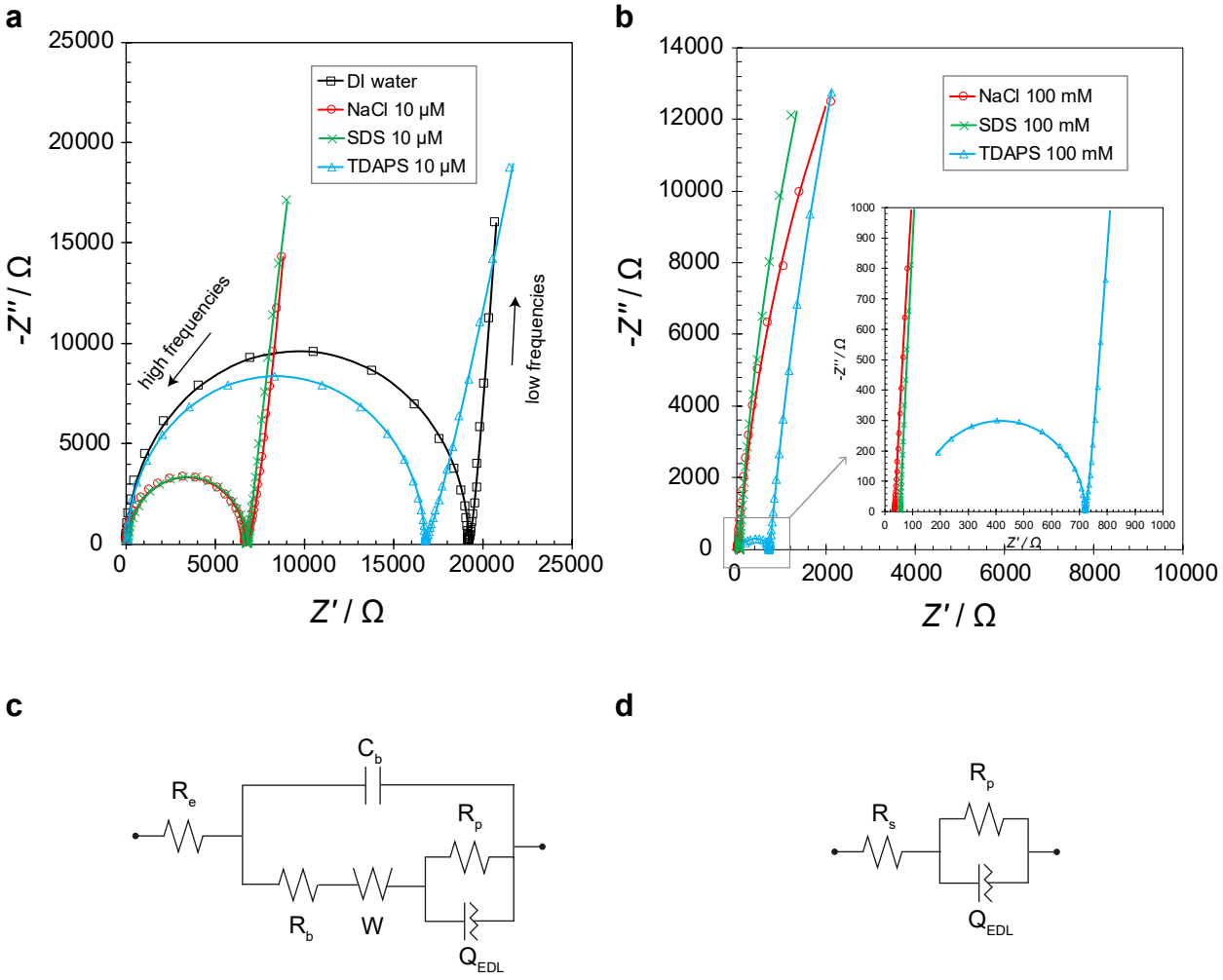

Figure 1: Nyquist plots for samples of (a) 10 μM and (b) 100 mM NaCl, SDS, and TDAPS in DI water. Equivalent circuits employed for regression of spectra (c) with and (d) without the bulk semicircle.

All spectra in Figure 1a have essentially the same shape and we can distinguish between two main regions: (i) the semicircle related to the liquid bulk phenomena and (ii) the tail-like segment of another semi-circle related to the EDL phenomena. The fact that we do not observe a full EDL semi-circle, is related to the absence of electrochemical reactions at the electrodes. As expected, the largest bulk semicircle is observed for pure DI water since the electrical resistivity determines the diameter of the semicircle. The sample containing 10 μM TDAPS also shows a relatively-larger semicircle compared to the NaCl and SDS samples. A zwitterionic surfactant does not carry a net charge. Therefore, the addition of small concentrations of TDAPS to DI water hardly changes the conductivity of the sample. [26] Further inspection shows that there is only a little difference between the samples containing NaCl and SDS. Nonetheless, the addition of the same amount of SDS or NaCl increases the electrical conductivity by almost 4 times compared to TDAPS.

A suitable equivalent circuit for regression of the spectra in Figure 1a is given in Figure 1c. The liquid bulk semicircle starts at the intersection with the x-axis at high frequencies. Here, the impedance of the system behaves like an ideal resistor (R_e in Figure 1c) and represents the ohmic resistances of wires and electrodes. When the frequency decreases, the capacitive characteristic of the liquid bulk triggers an impedance consisting of a real and an imaginary part which forms the semicircle. These characteristics are typically modelled using a parallel combination of a resistor and a capacitor (R_b and C_b in Figure 1c, respectively). At medium frequencies, we find the second intersection with the x-axis. The corresponding ohmic resistance is related to the sum of R_e and the liquid bulk resistance R_b. These resistances are often grouped as $R_s = R_e + R_b$, which is the total ohmic resistance in series with the elements that represent the EDL. At lower frequencies, the tail-like impedance related to the EDL appears in the spectrum. This part can also be divided into two subregions representing the transport phenomena and the capacitive effect. Please note that despite the lack of redox reactions at the electrodes, a charge transfer resistance must still be included in the circuit modelling since it influences the features of the tail-like impedance. The

representation of this EDL part can be made with a variety of approaches including (i) a single capacitor,[27–29] (ii) a parallel configuration of a capacitor and a resistor to account for the charge transfer (interfacial) resistance R_p,[28,30,31] and (iii) a parallel configuration of R_p and a constant phase element (CPE) to account for a capacitor with a distribution of time constants on the electrode surface.[32–37] In this work, we use a modification of the latter approach. It should be noted that since both electrodes in the measurement cell are similar, we assume both have the same impedance response. Hence, a single CPE (Q_{EDL}) and a charge transfer resistor R_p is used for the interpretation of the EDL effect of both electrodes. The calculated corresponding capacitance is then multiplied by two for the capacitance of a single electrode. In addition, we use a Warburg element in series with the EDL elements and the bulk resistance. The appearance of the Warburg element in systems without electrochemical reactions can be attributed to varying mobilities of the charge carriers.[6,25] This results in a diffusive transport of more mobile ion species in the liquid bulk in order to mitigate the effect of less mobile ions.[25]

Figure 1b shows the Nyquist plots for a solute concentration of 100 mM in DI water. At these relatively-high concentrations, the bulk liquid semicircles of the aqueous NaCl and SDS solutions are not observed anymore. This is due to the increased ionic conductivity and the influence of the inductive effects of wires and electrodes. However, in case of TDAPS, the semicircle is still visible since the addition of TDAPS hardly increases the conductivity. The addition of ionic species to the system has another profound influence. The transport effects become negligible compared to the liquid bulk resistance as the Debye length decreases.[25] Hence, above a certain concentration of NaCl and SDS, the utilization of a Warburg element is not suitable anymore. In addition, at higher concentrations, the tail-like EDL part of the NaCl spectrum has a lower slope compared to those in the SDS and TDAPS spectra. This is related to the lower charge transfer resistance of the NaCl sample which has a higher ionic strength. The regression of the spectra without the liquid bulk semicircle and without diffusion effects is based on the equivalent circuit shown in Figure 1d.

Admittance and Capacitance Spectra

As mentioned above, an impedance spectrum can be converted to an admittance or a capacitance spectrum using Equation (2) and Equation (3), respectively. The advantage of using these two quantities over the impedance is that they directly allow us to infer the EDL capacitance without further modelling assumptions.

Figure 2 gives the admittance and complex capacitance spectra for solutions with various concentrations of NaCl. The spectra for samples containing SDS and TDAPS are shown in the Supporting Information. Figure 2a shows the real part of the admittance over the excitation frequency. For all spectra, we see that $Y^{'}$ initially starts to increase with increasing frequency and arrives in a plateau-like behavior in the mid and high frequency range. This initial increase at low frequencies can be explained by inspecting the equivalent circuits. At the lowest frequencies, where we rather have DC conditions, the current has to pass all ohmic resistors including the relatively-large interface (charge transfer) resistance. If we increase the frequency, the current bypasses the charge transfer resistance via the EDL capacitor. In addition, the plateau-like region at mid to high frequencies represents the inverse value of R_s. Hence, the increase in the plateau from low to high concentrations is related to the increase in the liquid bulk conductivity.

Figure 2b gives the imaginary part of the complex admittance for different concentrations of NaCl. The low frequency slope of the correlation is slightly less than unity which confirms the appropriateness of a CPE for the equivalent circuit regression as discussed above. However, the main feature of these Y'' spectra is the presence of a characteristic frequency at the (local) maximum which is related to the EDL capacitance charging. We observe that the location of this maximum shifts towards higher frequencies as the NaCl concentration increases. In this context, it should be noted that this characteristic frequency cannot be retrieved from the impedance spectra for blocking electrodes. They are ideally modelled as a resistor in series with a capacitor R_sC_{EDL} and there is no local maximum in

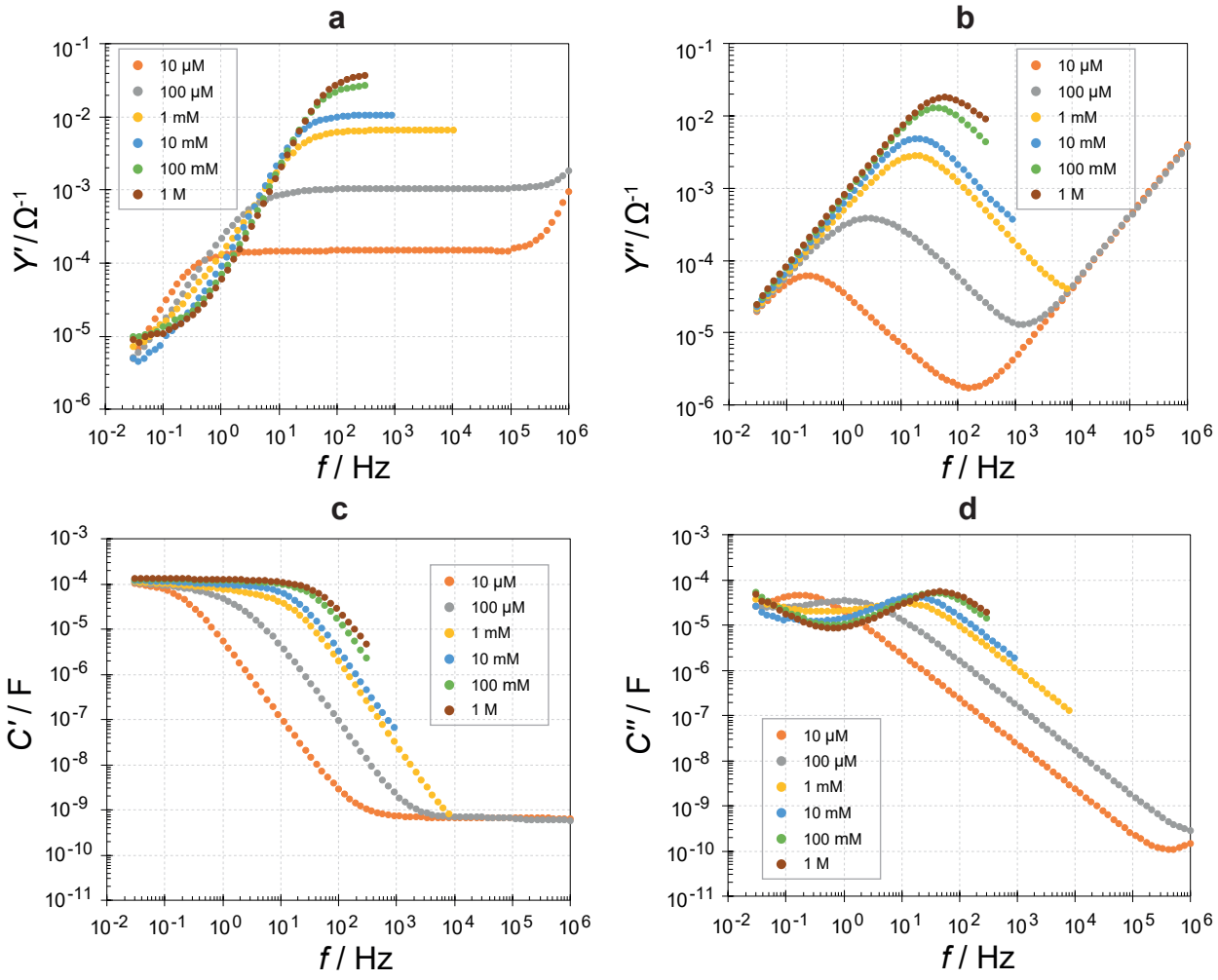

Figure 2: Complex admittance and capacitance spectra for different concentrations of NaCl: (a) real part of the admittance, (b) imaginary part of the admittance, (c) real part of the capacitance, and (d) imaginary part of the capacitance.

a $-Z''$ versus frequency plot to retrieve the characteristic frequency[24]. Likewise, for reactive electrodes, ideally modelled with $R_s(R_pC_{EDL})$, the characteristic frequency appears at a different frequency in the impedance spectra compared to admittance and capacitance spectra.[24] Therefore, we cannot employ the impedance spectrum for determining the capacitance unless we perform the regression to an equivalent circuit.

Figure 2c gives the real part of the complex capacitance versus the excitation frequency for samples with different NaCl concentrations. Generally, two plateau regions can be distinguished in the spectra. A high frequency plateau, which corresponds to the liquid bulk capacitance, can be seen for samples with a bulk semicircle in the impedance spectra. The bulk capacitance for the higher concentrations is not readily available due to inductive effects of the setup. The low frequency plateau, visible for all samples, has similar values for all concentrations, at least on a log-log scale. With the assumption of an ideal capacitive behavior, the low frequency plateau corresponds, for both blocking and reactive electrodes, to the EDL capacitance.[24] Therefore, we consider the low frequency plateau value of C' as a good approximation of the EDL capacitance.

Figure 2d shows the imaginary part of the complex capacitance spectrum. In the low to mid range, depending on the NaCl concentration, a characteristic frequency can be observed. This characteristic frequency is the same as in Figure 2b. However, an important aspect of the present plot is that it allows us to distinguish between blocking and reactive electrodes. A blocking electrode shows only a local maximum at low frequencies. A reactive electrode shows a local maximum followed by a local minimum at low frequencies.[24] In our system, the increase of C'' at lower frequencies can be seen for the samples with concentrations higher than 10 mM NaCl. Since this increase is not very significant it clarifies that we have a pseudo-blocking electrode system.

Electrical Double Layer Capacitance

In this section, we present the detailed processes to extract the EDL capacitance. First, we discuss the characteristic frequency and then the equivalent circuit regression approach. The results of both approaches are compared. Then, we present results and theoretical considerations for electrodes in aqueous electrolytes and in aqueous surfactant solutions.

For an ideal blocking electrode, the characteristic frequency f_0 of the admittance/capacitance spectrum is the frequency where the (local) maximum appears.[24] This frequency can be related to C_{EDL} and R_s according to

$$f_0 = \frac{1}{2\pi R_s C_{EDL}}. \tag{4}$$

For an ideal reactive electrode, f_0 does not exactly match the maximum in the Y'' or C'' spectrum.[24] In this case, f_0 is related to R_s, R_p and C_{EDL} according to

$$f_0 = \frac{1 + \frac{R_s}{R_p}}{2\pi R_s C_{EDL}}. \tag{5}$$

The electrodes in this study have a large charge transfer resistance and it is always $R_s/R_p < 0.001$ indicating non-ideal blocking electrodes. Note that comparison of Equation (5) and Equation (4) shows that for such cases both expressions are equivalent. In other words, for systems with a large charge transfer resistance, the relaxation frequency in the admittance/capacitance spectrum is controlled by the smaller resistance. In contrast, the relaxation frequency is controlled by the larger resistance in an impedance spectrum.[24] In this work, we extract R_s from the real part and f_0 from the imaginary part of the admittance spectrum, and employ Equation (4) to calculate the EDL capacitance.

The second approach to determine the EDL capacitance is based on the regression of an equivalent circuit to the impedance spectra. As discussed above, a CPE is usually employed to model the capacitive effects in the EDL since this element can compensate the impact of the distributed time constants. The impedance of a CPE corresponds to $1/Q_0(j\omega)^n$, where Q_0 is the CPE coefficient and the exponent is in the range of $0 \leq n \leq 1$. When $n = 1$, the CPE has the same characteristics as an ideal capacitor. For values of n close to 1, say $n > 0.8$, different relationships can be engaged to extract the equivalent capacitance of a CPE depending on whether there is a planar or normal distribution of the time constants along the electrode surface.[35,38,39] In our system, the electrode surface is considered as a single conductive layer with a planar distribution. Therefore, we use the approach of Brug et al.[32,39] to obtain the equivalent capacitance C_{EDL} according to

$$C_{EDL} = 2Q_0^{1/n} \left(\frac{R_s R_p}{R_s + R_p} \right)^{\frac{1-n}{n}} . \tag{6}$$

Since $R_p >> R_s$, Equation (6) can be simplified to

$$C_{EDL} = 2Q_0^{1/n} R_s^{\frac{1-n}{n}} . \tag{7}$$

To summarize, we fit the appropriate equivalent circuit, as given in Figure 1c or d, to the impedance spectra and use the respective regression values along with Equation (7) to infer the EDL capacitance. We compare this EDL capacitance with the results of the characteristic frequency method in order to validate the equivalent circuit approach.

Capacitance in Aqueous Electrolyte Solutions

Figure 3 gives the EDL capacitances which are inferred from both methods. It is striking that despite a NaCl concentration range over six orders of magnitude, the EDL capacitance

changes only to a limited extent. In general, all the capacitance values range from around 6 - 12 μF/cm^2 and both methods give the same trend and very similar values. The EDL capacitance, depending on the evaluation method, corresponds to around 9 - 11 μF/cm^2 for the lowest NaCl concentration. The capacitance drops with increasing concentration to a minimum value which is located at around 1 mM. Then, the capacitance increases with a further increase of the NaCl content. These EDL capacitance values are in good agreement with the most common range of EDL capacitance reported in literature, i.e., 5 - 20 μF/cm^2.[23] Additionally, we measure the EDL capacitance with CV, the results can be found in the Supporting Information to this article. When we plot the electrode capacitance vs. the electrolyte concentration from CV, we clearly observe the same trend, with the minimum located around 1 mM, as in the EIS results.

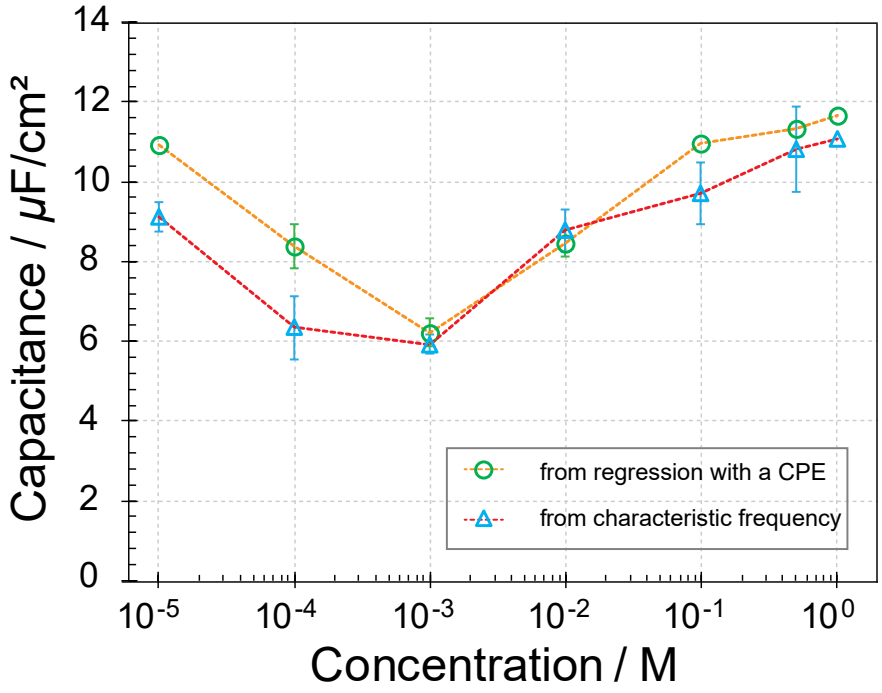

Figure 3: Electrical double layer capacitance from different evaluation methods vs. the NaCl concentration in the solution. Dashed lines are guides to the eye.

However, this observed behavior between capacitance and electrolyte concentration is not in agreement with the GC diffuse layer theory which predicts a steady capacitance increase for an increase of the electrolyte content as we further discuss below. In terms of

the GCS model, the overall capacitance of an EDL is the combination of two capacitors in series; i.e., the Stern layer C_{SL} and the diffuse layer C_{DL} capacitor[2,6,13] according to

$$\frac{1}{C_{EDL}} = \frac{1}{C_{SL}} + \frac{1}{C_{DL}}. \tag{8}$$

The capacitance of the SL can be expressed considering the capacity of an equivalent parallel plate capacitor as

$$C_{SL} = \frac{\varepsilon_{r,SL}\,\varepsilon_0 A}{l_{SL}}. \tag{9}$$

Here, ε_0 is the permittivity of the vacuum, $\varepsilon_{r,SL}$ and l_{SL} are the relative permittivity and the thickness of the SL, and A is the electrode area. Likewise, for a relatively low potential drop across the DL, its equivalent capacitance can be written as

$$C_{DL} = \frac{\varepsilon_r \varepsilon_0 A}{l_D}, \tag{10}$$

where ε_r is the relative permittivity in the DL, which is generally considered to be the same as the bulk permittivity, and l_D is the approximate thickness of the equivalent parallel plate capacitor. The Debye length

$$l_D = \sqrt{\frac{\varepsilon_r \varepsilon_0 RT}{2F^2 I}} \tag{11}$$

is generally used as the parameter for the DL thickness where R is the universal gas constant, T is the temperature, F is the Faraday constant, and $I = 0.5 \sum_i z_i^2 c_i$ is the ionic strength utilizing valency z_i and concentration c_i of the ionic species i. According to Equations (10) and (11), the Debye length varies with the square root of the inverse ionic strength. Therefore, the DL capacitance should increase proportionally with the square root of the electrolyte concentration.

In the following, we make some theoretical considerations in order to explain the ob-

served behavior between capacitance and electrolyte concentration. At first, we use correlations and data provided in ref.[40] and calculate the change in the bulk permittivity over the entire NaCl concentration range of our samples. We realize that this change is relatively minor and also does not have a significant effect on the calculation of the Debye length, the variation is less than 10%. Since the electric field in the DL is at least one order of magnitude lower than in the SL (see discussion below), the value of the liquid bulk permittivity $\varepsilon_r = 78.5$ can be used in the DL.[41,42] We now use Equation (10) and Equation (11) to calculate the theoretical DL capacitances C_{DL} over the entire range of concentrations. These DL capacitances are given in Figure 4 as curve a along with the measured electrode capacitances (open circles). We choose a log-log plot since the correlation of the DL capacitance with the concentration is then linear with a slope of 1/2. We notice that this theoretical DL capacitance increases from around 1 μF/cm^2 at 10 μM to more than 100 μF/cm^2 at 1 M concentration. That is, the change is three orders of magnitude which is in contrast to the experimental data that hardly vary (on a log-log axis).

The other capacitance that needs to be considered is the SL capacitance, which is more difficult to estimate. On the one hand, the thickness of the SL is not readily available by experimental methods. We estimate the SL thickness to be around 6 Å. This is based on the radius of a hydrated Na^+ and Cl^- (3 to 4 Å)[43,44] and the diameter of a water molecule (around 3 Å)[43] since this is the closest distance of an hydrated ion to the electrode surface. This value is consistent with the range of 3 to 10 Å that is given in literature.[45–49] On the other hand, the permittivity of the SL is unknown. Often, the permittivity in the entire EDL is assumed to be constant and equal to the permittivity of the liquid bulk.[50] However, the presence of the high electric fields in the SL ($\gtrsim 10^7$ V/m even for a low potential drop of 10 mV) considerably reduces the permittivity of water.[9,9,9,42,46,50–55] This reduction is related to the reorientation of the water molecules in order to compensate the high local electric field.[51] In addition, the water molecules are depleted since counter-ions are accumulated on the surface which also lowers the permittivity.[55,56] This can result in permittivities as low as

the saturation permittivity of water which is around 6.[19,57,58] The exact reduction is related to the surface charge density, zeta potential and the nature of electrolyte and electrode,[59] and is also a function of the distance from the surface.[50–52,60,61]

To summarize, we have no means to infer the exact thickness and permittivity of the SL but we definitely can use approximations which are on the right order of magnitude. For the further treatise, we combine these values and introduce the ratio of the relative permittivity in the SL to its thickness in angstrom, i.e., $\Pi \equiv \frac{\varepsilon_{r,SL}}{l_{SL}/\text{Å}}$. We now perform a scale (order of magnitude) analysis, where we assume the SL thickness to be similar to l_{SL} ∼10 Å. Then, the case of a reduced SL permittivity results in $\Pi = \frac{6}{10} \sim 1$ and the case of a non-reduced SL permittivity gives $\Pi = \frac{78.5}{10} \sim 10$. We compute the respective SL capacitances C_{SL} over the entire electrolyte concentration and add the results for $\Pi = 10$ and 1 to Figure 4 as curve b and c, respectively. Likewise, we use Equation (8) to compute the EDL capacitance C_{EDL} according to the GCS model as a combination of DL and SL capacitances; the values for $\Pi = 10$ and 1 are given as curve d and e, respectively.

As can be seen in Figure 4, the theoretical DL capacitance (curve a) increases from around 1 $\mu F/cm^2$ to around 200 $\mu F/cm^2$ over the entire concentration range. Both SL capacitances do not change over the concentration, but the non-reduced permittivity SL (curve b) capacitance is one order of magnitude higher than the reduced permittivity SL capacitance (curve c). The overall EDL (GCS) capacitance for both, non-reduced (curve d) and reduced permittivity (curve e), starts from the DL capacitance at very low concentrations and approaches the corresponding SL capacitance at very high concentrations. When we compare the experimental results with the theoretical predictions, we find that only the concept of a sole SL capacitance with reduced permittivity (curve c) gives a good agreement over the entire concentration range. In terms of the GCS model, the EDL capacitance assuming a reduced permittivity in the SL (curve e) is able to describe the experimental results at concentrations around 1 mM and higher, but there is significant disagreement

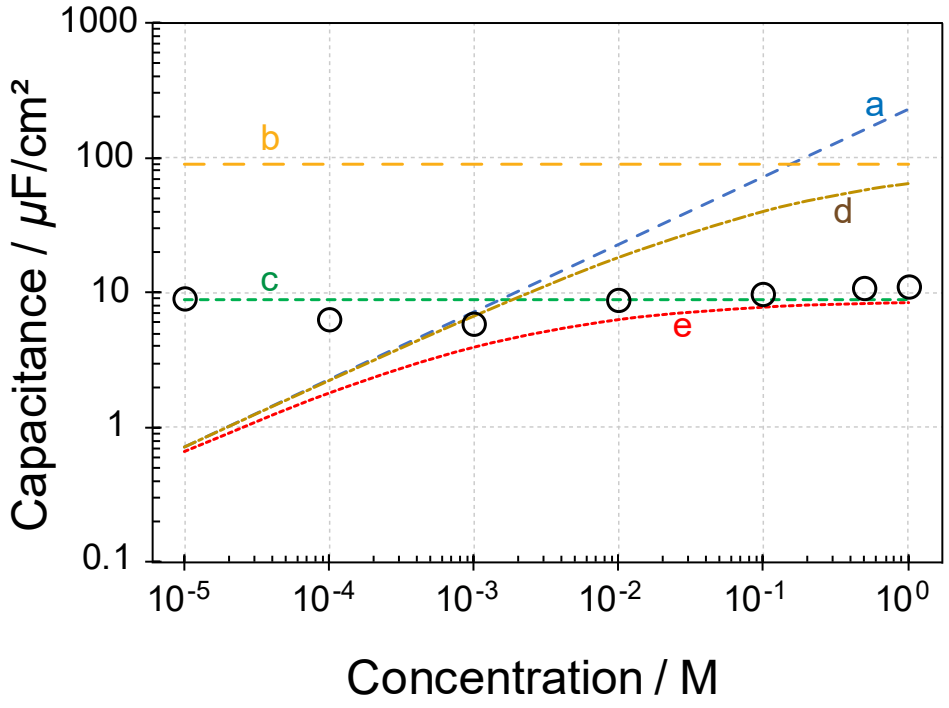

Figure 4: Capacitance versus NaCl concentration from experiment (open circles) and theory (curves): (a) diffuse layer capacitance C_{DL}; (b) Stern layer capacitance C_{SL} for $\Pi = 10$; (c) Stern layer capacitance C_{SL} for $\Pi = 1$; (d) EDL capacitance C_{EDL} for $\Pi = 10$; and (e) EDL capacitance C_{EDL} for $\Pi = 1$.

for lower concentrations. The serial arrangement of SL and DL capacitor requires that the smaller capacitor controls the behavior for the two capacitors. For the GCS model, the SL capacitor dominates at the high concentrations, while at low concentrations the DL capacitor should be in control. Thus, the agreement of curve c and e with the experimental data at high concentrations is a strong indication for a reduced permittivity in the SL. However, it is surprising that the sole reduced-permittivity SL capacitor still gives good agreement with the experiments at the very low concentrations while all models using a DL capacitor approach fail here. At very low ion concentrations, the Debye length is relatively large while the difference in ion density over the DL – the charge separation – is rather small. Furthermore, Khannanov et al.[62] experimentally showed that the length of the concentration gradient in the DL can be longer than theoretically predicted which further diminishes the capacitance. It seems that for these conditions the concept of a capacitor does not apply to the DL anymore. In other words, a measurable DL (capacitance) requires a sufficiently high ion gradient outside of the SL which is only established above a certain (minimum) ion concentration in the liquid. This hypothesis can also explain the drop in the measured capacitance between 10 μM and 1 mM (cf. Figure 3). In this range, the ion gradient outside the SL increases. This ion gradient is not enough to establish a measurable DL capacitor but rather lowers the capacitance of the SL due to a "smearing" of the Stern layer; an increase of the distance of the charge separation. When the DL capacitor is established, around 1 mM, any increase in ionic content lowers the Debye length which increases the DL capacitance so that the overall capacitor is controlled by the SL capacitor.

A regression results that a SL capacitance with $\Pi = 1.4$ gives the best agreement with the experimental results in Figure 4; this requires a relative permittivity of around 4 to 14 for an SL thickness in the range of 3 to 10 Å. This range corresponds very well with the saturation permittivity of water as discussed above. The corresponding SL capacitance for $\Pi = 1.4$ is 12 μF/cm^2. Since this value hardly changes over the entire concentration range, we apply Equation (8) and Equation (10) to infer the DL capacitance and Debye length from

the measured EDL capacitance, respectively. Figure 5 compares this "experimental" Debye length with the theoretical Debye length from Equation (11) over the entire concentration range of NaCl. As expected, a very good agreement is observed for NaCl concentrations above 1 mM. Considerable differences are obvious for the very low concentrations which again implies that a certain minimum ion content is required to form a diffuse layer which has characteristics according to the Gouy-Chapman theory. At low concentrations, only the SL capacitor seems to be dominant. Hence, calculation of the Debye length (i.e. the electrode distance of an equivalent parallel plate capacitor) from measured capacitances for concentrations below 1 mM should be avoided.

Similar deviations from the Gouy-Chapman-Stern model at low ion concentrations were previously observed in the impedance spectra of electrodes in aqueous HCl solutions[22]. Likewise, since an EDL has a different composition than the liquid bulk, it is possible to express its characteristics with the integral surface conductivity. In our previous work, we combined streaming current/potential and EIS measurements, and showed that Bikerman's correlation for the surface conductivity, which is based on the Gouy-Chapman model, fails at very low ion concentrations.[31] Furthermore, changes in the sign of the slope (inflection points) in correlations between absolute zeta potential and ionic strength at or below around 1 mM were reported in various works.[64–66] The zeta potential and the diffuse layer also determines the behavior of nanobubbles; here, Meegoda et al. observe an anomaly in nanobubble size at an ionic strength of around 1 mM which may be related to the lack/diminishment of the DL.[63] All these observations indicate that the conventional EDL theory fails to predict the behavior of the system at very low ionic strengths.

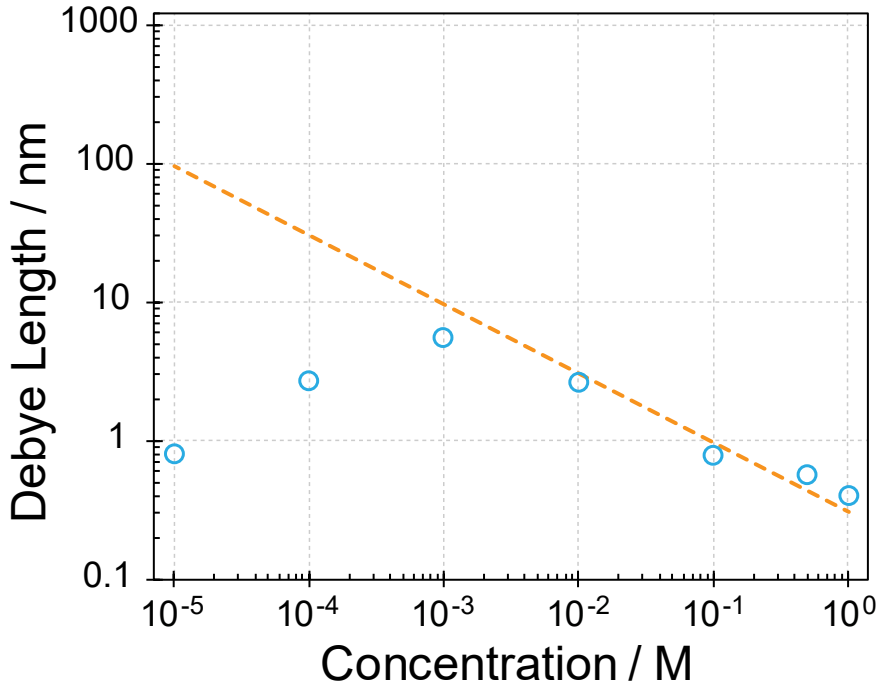

Figure 5: Comparison of experimental and theoretical Debye length versus the concentration (ionic strength) of NaCl. Open circles are experimental data while dashed line is based on theory.

Capacitance in Aqueous Surfactant Solutions

In the previous section, it is discussed that the EDL capacitance is always on the order of magnitude of the SL capacitance even for very low electrolyte concentrations. We further investigate this insignificance of the DL capacitance by performing measurements employing samples consisting of aqueous anionic SDS and zwitterionic TDAPS solutions. The main differences between a surfactant and a simple electrolyte, such as NaCl, is the size of the charge carrier. Surfactants are large molecules and form charged aggregates called micelles above the so-called critical micelle concentration (CMC).[67] Hence, in surfactant solutions the size of the charge carriers is much larger resulting in diffusivities which are considerably lower compared to simple electrolytes. Likewise, due to the aggregation process it is possible to have very low concentrations of large charge carrier. The micelles still form a Stern (adsorbed) layer due to electrostatic and/or other interactions such as hydrophobic adsorption.[26] However, this SL would be considerably thicker than in an aqueous electrolyte

so that electrostatic interactions outside of the SL are diminished and, in conjunction with the lower diffusivity (thermal energy), it is less likely to measure a DL capacitance. The entire EDL capacitance in a surfactant solution should be the SL capacitance, especially in the case of a zwitterionic surfactant which have no (integral) net charge.

We perform similar EIS measurements for SDS and TDAPS solutions in the concentration range of 10 μM - 100 mM of the surfactants. The spectra are fitted, depending on the presence or absence of the liquid bulk semicircle, to the equivalent circuits shown in Figure 1 c and d, respectively. The respective admittance and capacitance spectra and the regression results can be found in the Supporting Information. The equivalent EDL capacitances are then calculated based on the value of the CPE along with Equation (7). It should be noted that the ionic strength of a surfactant solution is correlated to the surfactant concentration in a much more complex way compared to a simple electrolyte. On the one hand, the zwitterionic TDAPS does not carry a net charge which makes the determination of an ionic strength difficult. On the other hand, the ionic strength of an SDS solution depends on the concentration of free surfactant molecules, degree of dissociation of the surfactant, and, for concentrations above CMC, on the micelle number density and aggregation number.[68] Hence, we plot the EDL capacitance versus the surfactant concentration in Figure 6. Both surfactants have an equal maximum concentration of 100 mM, which is close to their solubility limits. From conductivity data retrieved from the liquid bulk semicircle, along with a micelle size of around 5 nm measured with Direct Light Scattering, we can estimate the ionic strength of TDAPS for the highest concentration to be $\sim$1 mM. According to the analysis provided in our previous work,[68] the solution with the highest SDS concentration has an ionic strength of $\sim$10 mM. As it can be seen in Figure 6, both surfactants solutions result in very similar EDL capacitances of around 9 to 11 $\mu F/cm^2$. These values are on the same order of magnitude as the electrodes capacitances in the aqueous NaCl electrolytes. However, in contrast to the aqueous electrolyte we do not observe a significant change over the surfactant concentration. For the aqueous electrolyte, the capacitance dropped over

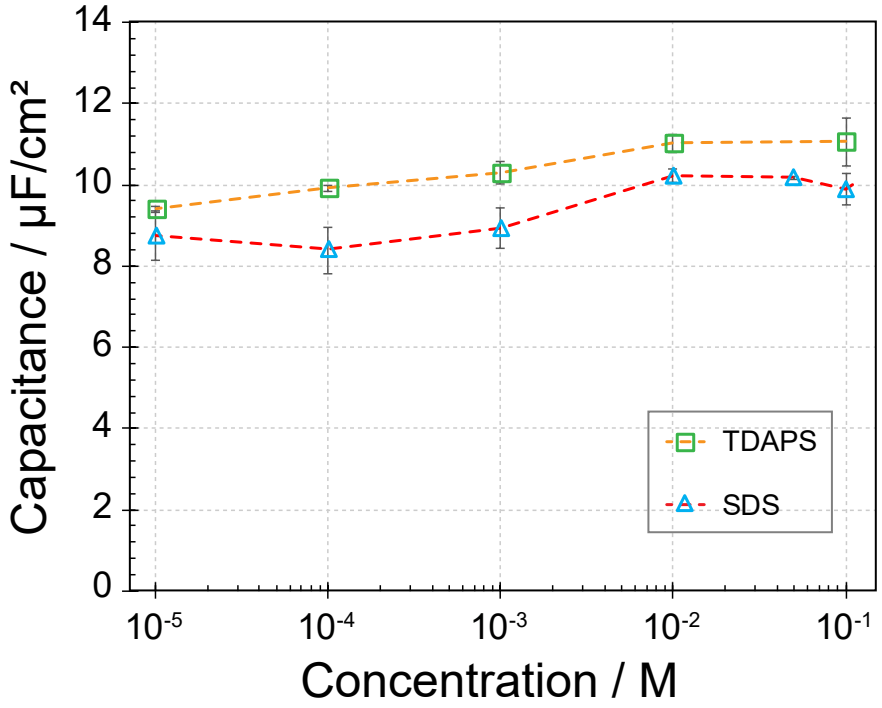

Figure 6: Electrical double layer capacitance vs. surfactant concentration. The maximum concentrations of TDAPS and SDS correspond to ionic strengths of roughly 1 mM and 10 mM, respectively. Dashed lines are guides to the eye.

the a comparable range of ionic strength, which is likely related to the change of the SL capacitor due to formation of the DL capacitor. In case of surfactant solutions, no drop is observed; we rather see a very minor increase of the capacitance. This is an indication that a DL (capacitor) in the traditional sense is not established in this range of low ionic strengths. The minor increase of the capacitance can be related to an increased adsorption which increases the charge density in the SL. The observed behavior demonstrates that the SL for these surfactants and the electrolyte solutions are very similar. This is probably related to the rather low permittivity variation for increasing surfactants solutions. In our previous work,[26] a drop of less than 10% of the static permittivity was observed when 100 mM SDS or TDAPS was added to water. Together with the lack of a DL in the case of surfactant solutions, this supports our assumption provided in the previous section for the aqueous electrolyte samples: At very low ionic strength, the ion gradient outside of the SL is not sufficient to establish a measurable DL (capacitor) and the GCS model should not be

applied.

Summary

In this work, the electrical impedance of aqueous samples of NaCl, SDS and TDAPS is measured in a two electrode setup over wide range of frequencies. Different approaches are employed to extract the capacitance of the electrical double layer located at the interface of electrode and sample. In detail, we use approaches based on equivalent circuits and, for the sake of validation, the characteristic relaxation frequency. Both methods give almost the same results proving the correctness of the equivalent circuits for our purposes.

The EDL capacitance is modelled according to the Gouy-Chapman-Stern model as a combination of two capacitances in series; i.e., the capacitances of the Stern and the diffuse layer. It is found that the EDL capacitance does not significantly change over a wide range of solute concentrations. A scaling analysis reveals that the permittivity in the Stern layer of the aqueous electrolyte samples is close to the water saturation permittivity. However, the measured capacitances are always on the same order of magnitude as the Stern layer capacitance. While this is in agreement with the theory at ionic strengths, this constitutes a considerable deviation for very low ion concentrations. The serial arrangement of Stern and diffuse layer entails that the smaller capacitor controls the total capacitor. Our results and considerations imply that a minimum ionic strength is needed to observe the effect of the diffuse layer on the overall EDL capacitance. We use the experimental results also to compute the electrode distance of an equivalent parallel plate capacitor and compare it with the Debye length, which is a measure for the thickness of the diffuse layer. Again, we find good agreement for ionic strengths above but considerable difference below around 1 mM. Additional experiments are carried out with surfactant solutions because their nature should result in a suppression of the formation of a diffuse layer. The surfactant containing samples

result in very similar EDL capacitances as the aqueous electrolyte samples. No significant change in capacitance is observed, indicating that the EDL consists only of a Stern layer. This supports our hypothesis that a Gouy-Chapman-like diffuse layer in an aqueous electrolyte is only established above a certain (minimum) ion concentration of around 1 mM.

Acknowledgement

The authors thank E.I. DuPont Canada Co. and NSERC for financial support and Dr. Carlos Escobedo, Queen's University for use of the 3D printer.

References

(1) Grahame, D. C. The electrical double layer and the theory of electrocapillarity. *Chemical Reviews* **1947**, *41*, 441–501.

(2) Hunter, R. J. *Foundations of colloid science*; Oxford University Press, 2001; p 806.

(3) Delgado, A. V.; González-Caballero, F.; Hunter, R. J.; Koopal, L. K.; Lyklema, J. Measurement and interpretation of electrokinetic phenomena. *Journal of Colloid and Interface Science* **2007**, *309*, 194–224.

(4) González, A.; Goikolea, E.; Barrena, J. A.; Mysyk, R. Review on supercapacitors: Technologies and materials. *Renewable and Sustainable Energy Reviews* **2016**, *58*, 1189–1206.

(5) Sharma, P.; Bhatti, T. A review on electrochemical double-layer capacitors. *Energy Conversion and Management* **2010**, *51*, 2901–2912.

(6) Macdonald, J. R. Impedance spectroscopy and its use in analyzing the steady-state AC response of solid and liquid electrolytes. *Journal of Electroanalytical Chemistry* **1987**, *223*, 25–50.

(7) Helmholtz, H. Studien über electrische Grenzschichten. *Annalen der Physik und Chemie* **1879**, *243*, 337–382.

(8) Burt, R.; Birkett, G.; Zhao, X. S. A review of molecular modelling of electric double layer capacitors. *Phys. Chem. Chem. Phys* **2014**, *16*, 6519.

(9) De Levie, R. The structure of charged interfaces. *Sensors and Actuators* **1981**, *1*, 97–109.

(10) Lyklema, J.; van Leeuwen, H. P.; van Vliet, T.; Cazabat, A. M. A.-M.; de Keizer, A.; Bijsterbosch, B. H.; Fleer, G. J. G. J.; Cohen Stuart, M. A. *Fundamentals of interface and colloid science, volume II: Solid-liquid interfaces*; Academic Press, 1995.

(11) Grahame, D. C. Capacity of the electrical double layer between mercury and aqueous sodium fluoride. II. Effect of temperature and concentration. *Journal of the American Chemical Society* **1957**, *79*, 2093–2098.

(12) Grahame, D. C.; Parsons, R. Components of charge and potential in the inner region of the electrical double layer: Aqueous potassium chloride solutions in contact with mercury at 25Âř. *Journal of the American Chemical Society* **1961**, *83*, 1291–1296.

(13) Lyklema, J.; Overbeek, J. T. G. Electrochemistry of silver iodide the capacity of the double layer at the silver iodide-water interface. *Journal of Colloid Science* **1961**, *16*, 595–608.

(14) Davis, J. A.; James, R. O.; Leckie, J. O. Surface ionization and complexation at the oxide/water interface. I. Computation of electrical double layer properties in simple electrolytes. *Journal of Colloid And Interface Science* **1978**, *63*, 480–499.

(15) Samec, Z. Electrical double layer at the interface between two immiscible electrolyte solutions. *Chemical Reviews* **1988**, *88*, 617–632.

(16) Fokkink, L.; de Keizer, A.; Lyklema, J. Temperature dependence of the electrical double layer on oxides: Rutile and hematite. *Journal of Colloid and Interface Science* **1989**, *127*, 116–131.

(17) Ishimatsu, R.; Shigematsu, F.; Hakuto, T.; Nishi, N.; Kakiuchi, T. Structure of the electrical double layer on the aqueous solution side of the polarized interface between water and a room-temperature ionic liquid, tetrahexylammonium bis(trifluoromethylsulfonyl)imide. *Langmuir* **2007**, *23*, 925–929.

(18) Garrido, J. A.; Nowy, S.; Härtl, A.; Stutzmann, M. The diamond/aqueous electrolyte interface: An impedance investigation. *Langmuir* **2008**, *24*, 3897–3904.

(19) Hou, Y.; Aoki, K. J.; Chen, J.; Nishiumi, T. Solvent variables controlling electric double layer capacitance at the metal-solution interface. *Journal of Physical Chemistry C* **2014**, *118*, 10153–10158.

(20) Aoki, K. J.; Chen, J. Effects of the dipolar double layer on elemental electrode processes at micro- and macro-interfaces. *Faraday Discussions* **2018**, *210*, 219–234.

(21) Hou, Y.; Aoki, K. J.; Chen, J.; Nishiumi, T. Invariance of Double Layer Capacitance to Polarized Potential in Halide Solutions. *Universal Journal of Chemistry* **2013**, *1*, 162–169.

(22) Zhao, X.; Aoki, K. J.; Chen, J.; Nishiumi, T. Examination of the Gouy-Chapman theory for double layer capacitance in deionized latex suspensions. *RSC Advances* **2014**, *4*, 63171–63181.

(23) Béguin, F.; Frackowiak, E. In *Supercapacitors: Materials, systems, and applications*; Béguin, F., Frąckowiak, E., Eds.; Wiley-VCH Verlag GmbH & Co. KGaA, 2013.

(24) Orazem, M. E.; Tribollet, B. *Electrochemical Impedance Spectroscopy*; John Wiley & Sons: Hoboken, NJ, USA, 2008.

(25) Barsoukov, E., Macdonald, J. R., Eds. *Impedance spectroscopy : theory, experiment, and applications*; John Wiley & Sons, Inc.: Hoboken, NJ, USA, 2005.

(26) Khademi, M.; Wang, W.; Reitinger, W.; Barz, D. P. Zeta potential of poly(methyl methacrylate) (PMMA) in contact with aqueous electrolyte-surfactant solutions. *Langmuir* **2017**, *33*, 10473–10482.

(27) Barker, G. The equivalent circuit for the electrical double layer. *Journal of Electroanalytical Chemistry (1959)* **1966**, *12*, 495–503.

(28) Grahame, D. C. Properties of the electrical double layer at a mercury surface. II. The effect of frequency on the capacity and resistance of ideal polarized electrodes. *Journal of the American Chemical Society* **1946**, *68*, 301–310.

(29) Dickinson, E. J. F.; Compton, R. G. How well does simple RC circuit analysis describe diffuse double layer capacitance at smooth micro- and nanoelectrodes? *Journal of Electroanalytical Chemistry* **2011**, *655*, 23–31.

(30) Sharma, P.; Bhatti, T. A review on electrochemical double-layer capacitors. *Energy Conversion and Management* **2010**, *51*, 2901–2912.

(31) Saini, R.; Garg, A.; Barz, D. P. Streaming potential revisited: The influence of convection on the surface conductivity. *Langmuir* **2014**, *30*, 10950–10961.

(32) Brug, G. J.; van den Eeden, A. L.; Sluyters-Rehbach, M.; Sluyters, J. H. The analysis of electrode impedances complicated by the presence of a constant phase element. *Journal of Electroanalytical Chemistry* **1984**, *176*, 275–295.

(33) Zoltowski, P. On the electrical capacitance of interfaces exhibiting constant phase element behaviour. *Journal of Electroanalytical Chemistry* **1998**, *443*, 149–154.

(34) Sadkowski, A. On the ideal polarisability of electrodes displaying cpe-type capacitance dispersion. *Journal of Electroanalytical Chemistry* **2000**, *481*, 222–226.

(35) Hirschorn, B.; Orazem, M. E.; Tribollet, B.; Vivier, V.; Frateur, I.; Musiani, M. Determination of effective capacitance and film thickness from constant-phase-element parameters. *Electrochimica Acta* **2010**, *55*, 6218–6227.

(36) Kang, J.; Wen, J.; Jayaram, S. H.; Yu, A.; Wang, X. Development of an equivalent circuit model for electrochemical double layer capacitors (EDLCs) with distinct electrolytes. *Electrochimica Acta* **2014**, *115*, 587–598.

(37) Córdoba-Torres, P. Relationship between constant-phase element (CPE) parameters and physical properties of films with a distributed resistivity. *Electrochimica Acta* **2017**, *225*, 592–604.

(38) Lvovich, V. F. *Impedance spectroscopy: Applications to electrochemical and dielectric phenomena*; John Wiley & Sons, 2012.

(39) Orazem, M. E.; Frateur, I.; Tribollet, B.; Vivier, V.; Marcelin, S.; Pebere, N.; Bunge, A. L.; White, E. A.; Riemer, D. P.; Musiani, M. Dielectric properties of materials showing constant-phase-element (CPE) impedance response. *Journal of the Electrochemical Society* **2013**, *160*, C215–C225.

(40) Wang, P.; Anderko, A. Computation of dielectric constants of solvent mixtures and electrolyte solutions. *Fluid Phase Equilibria* **2001**, *186*, 103–122.

(41) Wang, H.; Varghese, J.; Pilon, L. Simulation of electric double layer capacitors with mesoporous electrodes: Effects of morphology and electrolyte permittivity. *Electrochimica Acta* **2011**, *56*, 6189–6197.

(42) Booth, F. The dielectric constant of water and the saturation effect. *The Journal of Chemical Physics* **1951**, *19*, 391–394.

(43) Israelachvili, J. N. *Intermolecular and Surface Forces: Third Edition*; Elsevier Inc., 2011; pp 1–676.

(44) Volkov, A. G.; Paula, S.; Deamer, D. W. Two mechanisms of permeation of small neutral molecules and hydrated ions across phospholipid bilayers. Bioelectrochemistry and Bioenergetics. 1997; pp 153–160.

(45) Velikonja, A.; Gongadze, E.; Kralj-Iglic, V.; Iglic, A. *Charge dependent capacitance of stern layer and capacitance of electrode/electrolyte interface*; 2014; Vol. 9; pp 5885–5894.

(46) Hiemstra, T. Variable charge and electrical double layer of mineral-water interfaces: Silver halides versus metal (Hydr)oxides. *Langmuir* **2012**, *28*, 15614–15623.

(47) Brown, M. A.; Abbas, Z.; Kleibert, A.; Green, R. G.; Goel, A.; May, S.; Squires, T. M. Determination of surface potential and electrical double-layer structure at the aqueous electrolyte-nanoparticle interface. *Physical Review X* **2016**, *6*.

(48) Bourg, I. C.; Lee, S. S.; Fenter, P.; Tournassat, C. Stern layer structure and energetics at mica-water interfaces. *Journal of Physical Chemistry C* **2017**, *121*, 9402–9412.

(49) Wang, H.; Pilon, L. Accurate simulations of electric double layer capacitance of ultramicroelectrodes. *Journal of Physical Chemistry C* **2011**, *115*, 16711–16719.

(50) Gongadze, E.; Velikonja, A.; Perutkova, Š.; Kramar, P.; Maček-Lebar, A.; Kralj-Iglič, V.; Iglič, A. Ions and water molecules in an electrolyte solution in contact with charged and dipolar surfaces. *Electrochimica Acta* **2014**, *126*, 42–60.

(51) Teschke, O.; Ceotto, G.; de Souza, E. F. Interfacial water dielectric-permittivity-profile measurements using atomic force microscopy. *Physical Review E - Statistical Physics, Plasmas, Fluids, and Related Interdisciplinary Topics* **2001**, *64*, 10.

(52) Teschke, O.; De Souza, E. F. Hydrophobic surfaces probed by atomic force microscopy. *Langmuir* **2003**, *19*, 5357–5365.

(53) Le, G.; Zhang, J. A general Poisson-Boltzmann model with position-dependent dielectric permittivity for electric double layer analysis. *Langmuir* **2011**, *27*, 5366–5370.

(54) Zarzycki, P.; Rosso, K. M. Molecular dynamics simulation of the AgCl/electrolyte interfacial capacity. *Journal of Physical Chemistry C* **2010**, *114*, 10019–10026.

(55) López-García, J. J.; Horno, J.; Grosse, C. Poisson-Boltzmann description of the electrical double layer including ion size effects. *Langmuir* **2011**, *27*, 13970–13974.

(56) Gongadze, E.; Iglič, A. Decrease of permittivity of an electrolyte solution near a charged surface due to saturation and excluded volume effects. *Bioelectrochemistry* **2012**, *87*, 199–203.

(57) Hiemstra, T.; Van Riemsdijk, W. Physical chemical interpretation of primary charging behaviour of metal (hydr) oxides. *Colloids and Surfaces* **1991**, *59*, 7–25.

(58) Aoki, K. J. Frequency-dependence of electric double layer capacitance without Faradaic reactions. *Journal of Electroanalytical Chemistry* **2016**, *779*, 117–125.

(59) Hunter, R. J. *Zeta potential in colloid science : principles and applications*; Academic Press, 1981; p 386.

(60) Conway, B. E.; Bockris, J. O.; Ammar, I. A. *The dielectric constant of the solution in the diffuse and Helmholtz double layers at a charged interface in aqueous solution*; 1951; Vol. 47; pp 756–766.

(61) Wander, M. C.; Clark, A. E. Structural and dielectric properties of quartz - water interfaces. *Journal of Physical Chemistry C* **2008**, *112*, 19986–19994.

(62) Khannanov, A.; Gareev, B.; Batalin, G.; Amirova, L. M.; Dimiev, A. M. Counterion Concentration Profiles at the Graphene Oxide/Water Interface. *Langmuir* **2019**, *35*, 13469–13479.

(64) Johnson, P. R. A comparison of streaming and microelectrophoresis methods for obtaining the ζ potential of granular porous media surfaces. *Journal of Colloid and Interface Science* **1999**, *209*, 264–267.

(65) Alkafeef, S. F.; Gochin, R. J.; Smith, A. L. Measurement of the electrokinetic potential at reservoir rock surfaces avoiding the effect of surface conductivity. Colloids and Surfaces A: Physicochemical and Engineering Aspects. 1999; pp 263–270.

(66) Zembala, M.; Adamczyk, Z. Measurements of streaming potential for mica covered by colloid particles. *Langmuir* **2000**, *16*, 1593–1601.

(63) Meegoda, J. N.; Hewage, S. A.; Batagoda, J. H. Application of the Diffused Double Layer Theory to Nanobubbles. *Langmuir* **2019**, *35*, 12100–12112.

(67) Myers, D. *Surfactant science and technology*; John Wiley & Sons, 2005.

(68) Khademi, M.; Barz, D. P. Dielectric relaxation spectroscopy of aqueous micellar electrolyte solutions: A novel application to infer Dukhin number and zeta potential of a micelle. *Electrophoresis* **2019**, *40*, 710–719.